Analyzing Circuits with Widely Separated Time Scales Using Numerical PDE Methods

Jaijeet Roychowdhury

Abstract—Widely separated time scales arise in many kinds of circuits, e.g., switched-capacitor filters, mixers, switching power converters, etc. Numerical solution of such circuits is often difficult, especially when strong nonlinearities are present. In this paper, we present a mathematical formulation and numerical methods for analyzing a broad class of such circuits or systems. The key idea is to use *multiple time variables*, which enable signals with widely separated rates of variation to be represented efficiently. This results in the transformation of differential equation descriptions of a system to partial differential ones, in effect decoupling different rates of variation from each other. Numerical methods can then be used to solve the partial differential equations (PDEs). In particular, time-domain methods can be used to handle the hitherto difficult case of strong nonlinearities together with widely separated rates of signal variation. We examine methods for obtaining quasi-periodic and envelope solutions, and describe how the PDE formulation unifies existing techniques for separated-time-constant problems. Several applications are described. Significant computation and memory savings result from using the new numerical techniques, which also scale gracefully with problem size.

Index Terms—Multitime partial differential equations, widely separated time scales.

I. INTRODUCTION

CONSIDER a 1-GHz pulse train multiplied with a 1-kHz sinusoid, or the same pulse train with the duty cycle of each pulse controlled by a slow information signal. These may be termed *multirate signals*, i.e., they contain "components" that vary at two or more widely separated rates. Such signals arise in various physical systems, such as communication circuits (e.g., up/down-converters, automatic gain-control circuits), cycle-chopping and switched power converters, switched-capacitor filters, pulsewidth-modulation circuits, etc. Such systems are typically difficult to analyze using traditional numerical integration algorithms, such as those in programs like SPICE [1], [2]. The difficulty stems from the widely disparate rates: following fast-varying signal components long enough to obtain information about the slowly-varying ones is computationally expensive, and can also be inaccurate. Furthermore, if the circuits are strongly nonlinear, specialized methods (see Section II) that can solve linear and mildly nonlinear circuits quickly become ineffective.

In this paper, we present a novel approach for analyzing such problems, using the fact that many multirate signals, especially from circuits, can be represented efficiently as functions of two or more time variables, i.e., as *multivariate functions*. If a system is described with differential-algebraic equations (DAEs), using multivariate functions for the unknowns leads naturally to a partial differential equation (PDE) form, which we call the *Multitime Partial Differential Equation (MPDE)*. By applying time-domain numerical methods to solve the MPDE directly for the multivariate forms of the unknowns, we are able to analyze the combination of strong nonlinearities and multirate signals.

The immediate advantage of this approach is that it can result in improvements in simulation speed compared to DAE-based alternatives—this is the main focus in this paper. The uses of the MPDE formulation are not, however, limited to numerical ones. For example, multiple time variables can be used to tag different inputs symbolically, even if nothing is known about the nature of the inputs' variations. This idea has been used to analyze and macromodel linear periodic time-varying (LPTV) systems [3]. Another use has been for autonomous systems, where the concept of instantaneous frequency has been extended to oscillators with arbitrary responses, and the oscillator equations recast to include the changing frequency as an explicit variable in the dynamical system description [4]. It is possible that further ways of analyzing dynamical systems, at higher levels of abstraction than previously possible, may result through use of the multitime concept.

II. PREVIOUS WORK

Awareness of the multiple time approach seems low in the circuits community, but the concept is not new and has apparently been rediscovered several times. Artificial-time multivariate functions and related PDE forms have been used for asymptotic expansion analysis [5] for decades, though only as analytical conveniences for certain simple, weakly nonlinear harmonic oscillators. Ngoya and Larchevèque [6] appear to have been first to recognize the value of multiple time scales in a more general context, and mention their relevance to envelope simulation. Most recently, Brachtendorf *et al.* [7] have used the PDE form to obtain a simple and elegant derivation of the multi-tone harmonic balance method described below.

A number of methods exist for numerical analysis of DAE systems with multirate signals. The simplest and most prevalent (e.g., in SPICE [1], [2]) employ time-stepping numerical DAE integration to solve an initial-value problem. As discussed in the next section, these have difficulty with multirate signals because time-steps need to be smaller than the period of the fastest signal component, leading to a large number of time-points for simulating the slowest component. Numerical errors can also build up significantly over the long simulation, even in the presence of tight local error control.
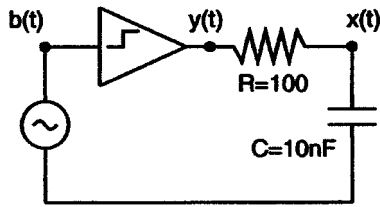
Fig. 1.   Two-tone input to comparator followed by *RC* filter.

Fig. 2.   Example two-tone quasi-periodic signal $b(t)$.

Fig. 3.   Corresponding two-periodic bivariate form $\hat{b}(t_1, t_2)$.

More effective, though limited largely to weakly nonlinear systems, is a frequency-domain technique for quasi-periodic signals known as Harmonic Balance (HB). In multi-tone harmonic balance (e.g., [8]–[10], [7]), an algebraic system of equations in the Fourier coefficients is set up and solved. Solving directly for the Fourier coefficients enables HB to circumvent the small time-step problem, but also hampers it in situations where waveforms cannot be represented with few Fourier components, e.g., in strongly nonlinear circuits containing waveforms with sharp edges and spikes. Another limitation of HB relates to the structure of its Jacobian matrix, which loses block-diagonal dominance as nonlinearities grow strong. Loss of diagonal dominance is significant because preconditioned iterative linear algebra techniques (e.g., [11], [9]), needed for solving large problems, become ineffective as diagonal dominance is lost.

Envelope-modulated signals can be analyzed using recent techniques [12], [13] that formulate the problem as a differential equation in the time-varying Fourier coefficients. Traditional time-stepping techniques are used to solve the differential equation, resulting in a smaller dimensional quasi-periodic system, solved using harmonic balance, at each time-point. The methods have some deficiencies: they are derived by equating the time-varying coefficients of two Fourier expansions, a procedure that is not strictly valid; also, the inner loop of these methods are based on HB, hence they share HBs disadvantages with respect to strong nonlinearities.

The nonlinearity limitation of harmonic balance can be partially overcome for an important special case of the quasi-periodic problem, by using the methods of Chua and Ushida [14] and Kundert *et al.* [15], [8]. Two relationships are set up and equated to form a nonlinear equation system, solving which provides the quasi-periodic response. One relationship is obtained from a transient simulation of the circuit ODEs over a few periods of the fast cycle, the other from the variation, over the fast periods, due to the slowly varying components of the signal, which are assumed to have short Fourier series expansions. This approach has been used to analyze distortion in switched-capacitor circuits, in which the signal path generates relatively few harmonics.

III. MULTILINE REPRESENTATIONS AND THEIR BENEFITS

The circuit of Fig. 1 consists of a comparator followed by an *RC* filter. The input to the comparator $b(t)$ (shown in Fig. 2) is a simple two-tone quasi-periodic signal given by

$$b(t) = \sin\left(\frac{2\pi}{T_1}t\right)\sin\left(\frac{2\pi}{T_2}t\right),$$
$$T_1 = 1\,\text{ms} \quad T_2 = 0.01\,\text{ms}. \tag{1}$$
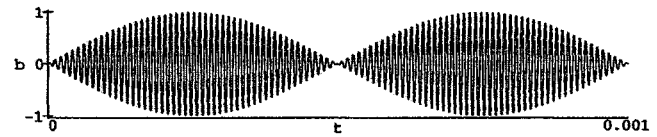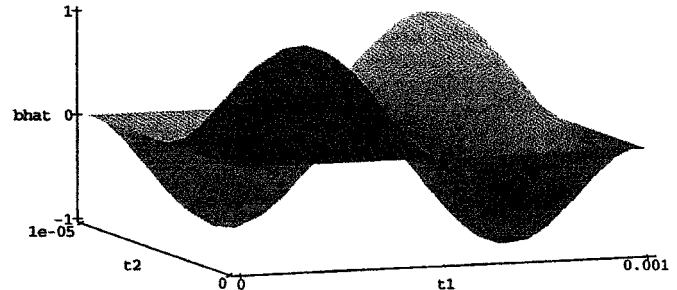
The two tones are at frequencies $f_1 = 1/T_1 = 1$ kHz and $f_2 = 1/T_2 = 100$ kHz. There are 100 fast-varying cycles of period $T_2 = 0.01$ ms modulated by a slowly-varying sinusoid of period $T_1 = 1$ ms.

Simulating the circuit using numerical integration schemes (i.e., transient or shooting analysis) would require time-steps spaced closely enough to represent each fast cycle in $b(t)$ accurately. If each cycle is sampled at n points, the total number of time-steps needed for one period of the slow modulation is $n(T_1/T_2)$. To generate Fig. 2, 15 points were used per cycle, hence the total number of samples was 1500. This number is proportional to the separation between the time scales, and can be much larger in, e.g., RF circuit applications.
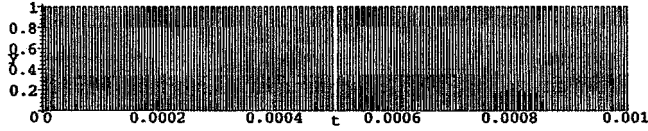
Now, consider a multi-time representation for $b(t)$, constructed as follows: for the "slowly-varying" parts of the expression for $b(t)$, t is replaced by t_1; for the "fast-varying" parts, by t_2. The resulting function of two variables is denoted by $\hat{b}(t_1, t_2)$

$$\hat{b}(t_1, t_2) = \sin\left(\frac{2\pi}{T_1}t_1\right)\sin\left(\frac{2\pi}{T_2}t_2\right). \tag{2}$$

Note, that $\hat{b}(t_1, t_2)$ is *biperiodic*, i.e., periodic with respect to both t_1 and t_2: $\hat{b}(t_1 + T_1, t_2 + T_2) = \hat{b}(t_1, t_2)$. The plot of $\hat{b}(t_1, t_2)$ on the rectangle $0 \le t_1 \le T_1$, $0 \le t_2 \le T_2$ is shown in Fig. 3. Because $\hat{b}$ is biperiodic, this plot repeats over the rest of the t_1–t_2 plane. Note, also that $\hat{b}(t_1, t_2)$ does not have many undulations, unlike $b(t)$ in Fig. 2. *Hence it can be represented using relatively few sample points.* Fig. 3 was plotted on a uniform 15×15 grid, i.e., 225 samples—far fewer than the 1500 points for Fig. 2.

Note, further that it is easy to recover $b(t)$ from $\hat{b}(t_1, t_2)$, simply by setting $t_1 = t_2 = t$, and using the fact that $\hat{b}$ is biperiodic. Given any value of t, the arguments to $\hat{b}$ are given by $t_i = t \bmod T_i$. For example

$$b(1.952\,\text{ms}) = \hat{b}(1.952\,\text{ms}, 1.952\,\text{ms})$$
$$= \hat{b}(T_1 + 0.952\,\text{ms}, 195T_2 + 0.002\,\text{ms})$$
$$= \hat{b}(0.952\,\text{ms}, 0.002\,\text{ms}).$$
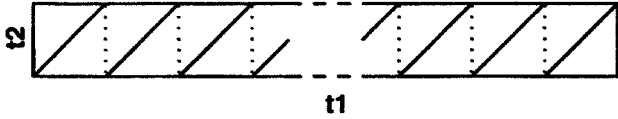
Fig. 4.   Path in the t_1–t_2 plane.

Fig. 5. $y(t)$.

Fig. 6. $\hat{y}(t_1, t_2)$.

Fig. 7. $\hat{x}(t_1, t_2)$.

Fig. 8. $x(t)$.
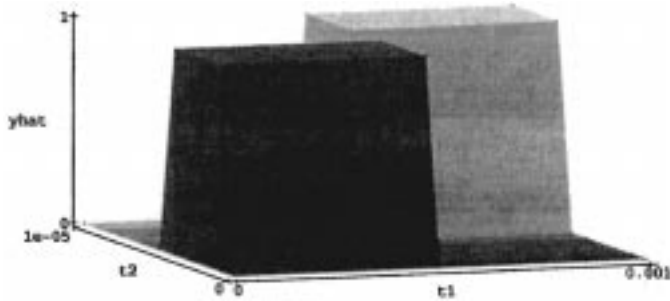
Given $\hat{b}(t_1, t_2)$, it is easy to visualize what $b(t)$ looks like. As t increases from 0, the path given by $\{t_i = t \bmod T_i\}$ traces the sawtooth path shown in Fig. 4. By noting how $\hat{b}$ changes as this path is traced, the behavior of $b(t)$ can be visualized. Variations of the bivariate waveform along the slow and fast time axes directly reflect the respective components of $y(t)$, more naturally and conveniently than $y(t)$ itself.

The above illustrates two important features: 1) the bivariate form can require far fewer points to represent numerically than the original quasi-periodic signal, yet 2) it contains all the information needed to recover the original signal completely. This is true not only for signals with a compact frequency-domain representation [such as $b(t)$ in (1), with only two frequency components, $f_2 \pm f_1$], but also for those that cannot be represented efficiently in the frequency domain. For example, consider the quasi-periodic digital signal $y(t)$ at the output of the comparator

$$y(t) = \mathrm{comp}(b(t)), \qquad \mathrm{comp}(z) \approx \begin{cases} 1 & \text{if } z > 0 \\ 0 & \text{otherwise.} \end{cases}$$

Representing $y(t)$ adequately in the frequency domain requires perhaps 625 Fourier coefficients, since at least 25 harmonics in each tone are needed to represent a square wave more or less accurately. As for the univariate time-domain representation, more than 400 points are needed, as shown in Fig. 5. However, the bivariate representation $\hat{y}(t_1, t_2)$, given by

$$\hat{y}(t_1, t_2) = \mathrm{comp}\left(\hat{b}(t_1, t_2)\right)$$

and plotted in Fig. 6, requires only about 40 points to represent accurately. As before, $y(t)$ is easily recoverable by the relation $y(t) = \hat{y}(t, t)$ and the biperiodicity of $\hat{y}$.
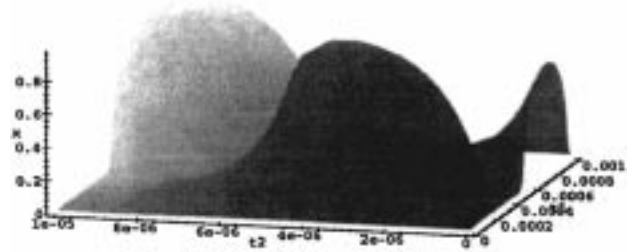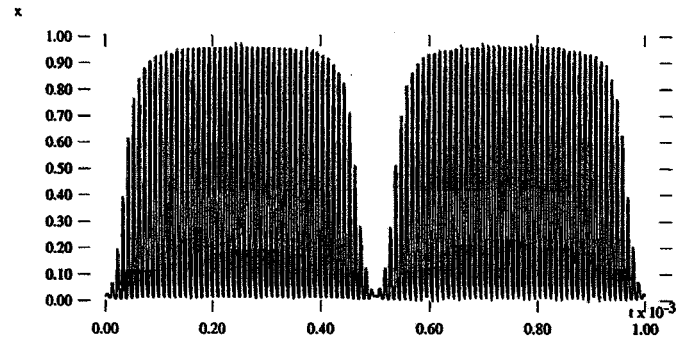
The key to the numerical techniques in this paper is to solve for the multivariate forms of all the node voltages and branch currents of a circuit directly. The details are presented in Sections IV and V. The basic notion is to rewrite the circuit's equations in terms of multivariate functions, in effect transforming the original differential equations into an MPDE. By applying boundary conditions (BCs) to the MPDE and solving it numerically with time-domain or mixed frequency-time methods, the multivariate solutions are obtained efficiently. If desired, the univariate solution of the circuit can be easily computed from the multivariate one; often, however, information of interest can be obtained directly by inspecting the multivariate solution.

For example, given the differential equation for the circuit of Fig. 1

$$\dot{x} = f(x, b) = \frac{\mathrm{comp}(b(t)) - x}{RC} \tag{3}$$

the corresponding MPDE can be shown to be (see Section IV)

$$\frac{\partial \hat{x}}{\partial t_1} + \frac{\partial \hat{x}}{\partial t_2} = f(\hat{x}, \hat{b}) = \frac{\mathrm{comp}\left(\hat{b}(t_1, t_2)\right) - \hat{x}(t_1, t_2)}{RC}. \tag{4}$$

The quasi-periodic steady state of the solution $\hat{x}(t_1, t_2)$ is captured by using *biperiodic BCs* for (4), i.e., $\hat{x}(t_1 + T_1, t_2 + T_2) = \hat{x}(t_1, t_2)$. The solution $\hat{x}(t_1, t_2)$, obtained using the methods described in Section V, is plotted in Fig. 7. The univariate solution $x(t)$, generated using $x(t) = \hat{x}(t, t)$, is plotted in Fig. 8. It is evident that, for a given accuracy, the bivariate form is much more compact than the univariate form. Moreover, the main features of interest, i.e., the slow scale variation of the rectified voltage, as well as the fast scale ripple, are immediately apparent from the variations along the slow and fast time axes of Fig. 7.

IV. THE MULTITIME PARTIAL DIFFERENTIAL EQUATION (MPDE) AND ITS PROPERTIES

In this section, the MPDE is examined (see also [5]–[7]). The connection between the MPDE and the circuit's DAE is explored first and the basic link between their solutions is proven. BCs leading to quasi-periodic and envelope-modulated solutions are presented next. Finally, it is shown why FM-type signals cannot be handled efficiently by the MPDE.

We start with a general DAE form of a circuit's equations

$$\dot{q}(x) = f(x) + b(t). \tag{5}$$

All variables (except the time t) are vector-valued. $x(t)$ are the unknowns in the circuit (node voltages and branch currents), q the charge terms, and f the resistive terms. $b(t)$ is the vector of excitations to the circuit (typically from independent voltage/current sources).

As discussed in Section III, if the circuit exhibits multirate behavior, its variables can often be represented efficiently using multiple time variables. If there are m separate rates of change, m time-scales are used. Denote the multivariate forms of $x(t)$ and $b(t)$ by $\hat{x}(t_1, \ldots, t_m)$ and $\hat{b}(t_1, \ldots, t_m)$. We proceed by first defining a PDE in these multivariate forms, and then showing how solutions of this equation generate solutions of (5). First, we define the MPDE corresponding to (5) to be

$$\frac{\partial q(\hat{x})}{\partial t_1} + \cdots + \frac{\partial q(\hat{x})}{\partial t_m} = f(\hat{x}) + \hat{b}(t_1, \ldots, t_m) \tag{6}$$

where f and q are the same functions as in (5).

We show next that there is a key relation between the MPDE and the circuit's DAEs. Theorem 1 states that solutions to the circuit's DAEs are available on "diagonal" lines along the MPDE's multivariate solutions. This is a completely general result; indeed, $x(t)$ or $b(t)$ need not exhibit any multirate behavior at all.

Theorem 1 (MPDE-DAE Relation): If $\hat{x}(t_1, \ldots, t_m)$ and $\hat{b}(t_1, \ldots, t_m)$ satisfy the MPDE in (6), then $x(t) = \hat{x}(t+c_1, \ldots, t+c_m)$ and $b(t) = \hat{b}(t+c_1, \ldots, t+c_m)$ satisfy the circuit's DAE in (5), for any fixed $c_1, \ldots, c_m$.

Proof: See the Appendix. ∎

To solve the MPDE, it is necessary to first specify BCs. Different BCs lead to quasi-periodic and envelope-modulated solutions.

A. Quasi-Periodic Signals

A signal is quasi-periodic if it satisfies the following definition [16].

Definition 1: $y(t)$ is *m-tone quasi-periodic* if it can be expressed in the form

$$y(t) = \sum_{i_1, \ldots, i_m} Y(i_1, \ldots, i_m)$$
$$\cdot \exp\left(j2\pi\left(\frac{i_1}{T_1} + \cdots + \frac{i_m}{T_m}\right)t\right)$$

where $Y(i_1, \ldots, i_m)$ are real- or complex-valued constants.

Quasi-periodicity for univariate signals is closely related to periodicity for multivariate signals.

Definition 2: A multivariate function $\hat{y}(t_1, \ldots, t_m)$ is *m-periodic* (or simply *periodic*) if $\hat{y}(t_1 + k_1T_1, \ldots, t_m + k_mT_m) = \hat{y}(t_1, \cdots, t_m)$ for all real $t_1, \ldots, t_m$ and all integers $k_1, \ldots, k_m$. $T_1, \ldots, T_m$ are constant real numbers; T_i is referred to as the *period of the ith tone of $\hat{y}$* or simply the *ith period of $\hat{y}$*.

The following two simple lemmas follow immediately from the previous definitions. Lemma 1 shows that given any periodic multivariate signal $\hat{y}$, a quasi-periodic signal y is immediately obtained by evaluating $\hat{y}$ on a diagonal line. Lemma 2 shows that given any quasi-periodic signal y, a periodic multivariate signal $\hat{y}$ can be found that satisfies Lemma 1.

Lemma 1: If $\hat{y}(t_1, \ldots, t_m)$ is m-periodic, then $y(t) = \hat{y}(t+c_1, \ldots, t+c_m)$ is m-tone quasi-periodic for any $c_1, \ldots, c_m$.

Proof: See the Appendix. ∎

Lemma 2: Given any m-tone quasi-periodic function $y(t)$ and any constants $c_1, \ldots, c_m$, an m-periodic $\hat{y}(t_1, \ldots, t_m)$ can be found that satisfies $y(t) = \hat{y}(t+c_1, \ldots, t+c_m)$.

Proof: See the Appendix. ∎

Applying the above lemmas to Theorem 1 results in the following theorem and corollary, which establish that any m-periodic solution of the MPDE generates a corresponding quasi-periodic solution of the circuit's DAEs. Hence, to generate a quasi-periodic solution, it is sufficient to 1) find a periodic $\hat{b}$ satisfying $\hat{b}(t+c_1, \ldots, t+c_m) = b(t)$ and 2) solve the MPDE with periodic BCs.

Theorem 2 (MPDE Sufficiency Condition): If $\hat{b}$ is an m-periodic excitation to (6) and $\hat{x}$ an m-periodic solution, then $x(t) = \hat{x}(t+c_1, \ldots, t+c_m)$ is an m-tone quasi-periodic solution of (5) under the m-tone quasi-periodic excitation $b(t) = \hat{b}(t+c_1, \ldots, t+c_m)$.

Corollary 1: Given an m-periodic $\hat{b}$ such that $b(t) = \hat{b}(t+c_1, \ldots, t+c_m)$, it is sufficient to find a solution $\hat{x}$ of the MPDE with m-periodic BCs in order to obtain an m-tone quasi-periodic solution $x(t) = \hat{x}(t+c_1, \ldots, t+c_m)$ of the circuit DAE.

Theorem 2 establishes a one-way link between the MPDE and DAE formulations, by showing that any periodic solution of the MPDE generates a quasi-periodic one for the DAE. The other direction is equally important, because it shows that if the original problem has a quasi-periodic solution, then the MPDE also has a corresponding solution; hence no solution of the original system is lost by moving to the MPDE formulation. This is established by the following theorem.

Theorem 3 (MPDE Necessity Condition): If a quasi-periodic solution $x(t)$ of the circuit DAE (5) exists for a quasi-periodic excitation $b(t)$, then for any $c_1, \ldots, c_m$, there exist m-periodic functions $\hat{b}(t_1, \ldots, t_m)$ and $\hat{x}(t_1, \ldots, t_m)$ satisfying the MPDE (6) such that $x(t) = \hat{x}(t+c_1, \ldots, t+c_m)$, $b(t) = \hat{b}(t+c_1, \ldots, t+c_m)$.

Proof: See the Appendix. ∎

The existence or uniqueness of a solution to the MPDE with periodic BCs cannot, in general, be guaranteed, just as the existence/uniqueness of quasi-periodic solutions for the circuit DAE cannot be guaranteed. This is easily verified by considering the equation $\dot{x} = 0$, which has an infinite number of (constant) periodic solutions, and the equation $\dot{x} = 1 + \cos(t)$, which has no quasi-periodic solutions at all.
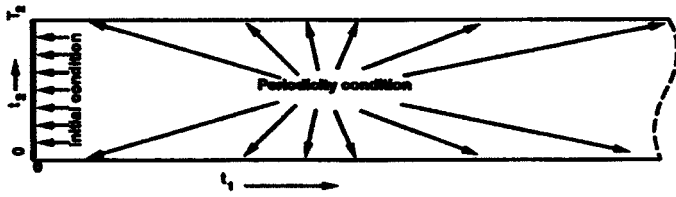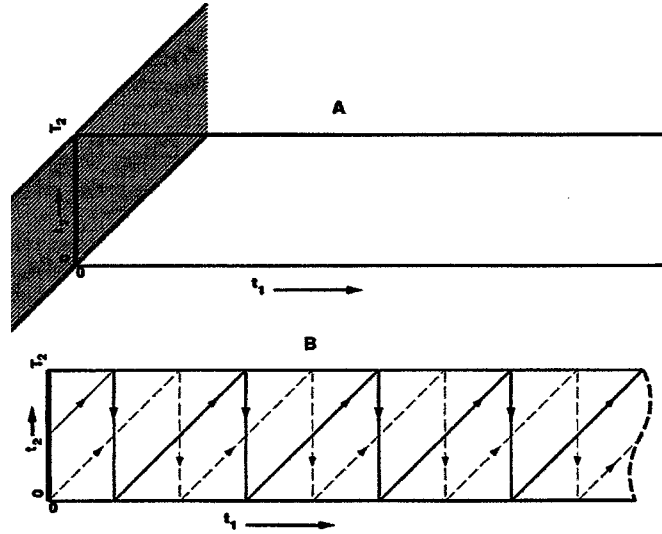
Fig. 9.   Envelope BCs.

Fig. 10.   Uniqueness of envelope solution.

B. Envelope-Modulated Signals

The multivariate form of an *envelope-modulated* or *envelope* signal with $m-1$ periodic components can be defined as

$$
\hat{x}(t_1, t_2, \ldots, t_m)
$$
$$
= \sum_{i_2, \ldots, i_m} X_{i_2, \ldots, i_m}(t_1)
$$
$$
\cdot \exp\left(j2\pi\left(i_2\frac{t_2}{T_2} + \cdots + i_m\frac{t_m}{T_m}\right)\right) \qquad (7)
$$

$\hat{x}$ is periodic with respect to each of its arguments except t_1, which is, in practical applications, the variable with the slowest rate. The univariate signal is therefore in the form of a Fourier series with time-varying coefficients (the envelopes).

Envelope solutions of the form of (7) correspond to a combination of initial and periodic BCs for the MPDE, illustrated for the two-rate case in Fig. 9. More precisely, the requirements are that: 1) $\hat{x}(0, t_2, \ldots, t_m)$ is specified, and 2) $\hat{x}$ is T_i-periodic with respect to each argument t_i. Given these conditions, the following theorem shows that the envelope solution is unique.

Theorem 4 (Uniqueness of Envelope): If the DAE (5) has a unique solution given any initial condition, the solution $\hat{x}(t_1, \ldots, t_m)$ of the MPDE is also unique, given the following mixed initial and periodic BCs

$$
\hat{x}(t_1, t_2 + T_2, \ldots, t_m + T_m) = \hat{x}(t_1, \ldots, t_m)
$$
$$
\hat{x}(0, t_2, \ldots, t_m) = h(t_2, \ldots, t_m)
$$

where h is any given initial-condition function, defined on $\prod_{i=2}^{m}[0, T_i]$.

Proof: See the Appendix.   ∎

Although the *multivariate* envelope solution is unique for a given initial condition on the $t_1 = 0$ line, there exist an infinite number of possible initial conditions that all generate exactly the same *univariate* solution. This is illustrated in Fig. 10(b). The univariate solution along the $t_1 = t_2$ line, for example, can be shown to be determined only by the value of the initial condition at $t_2 = 0$. The initial condition at other values of t_2 [e.g., at $(t_1 = 0, t_2 = T_2/2)$, as illustrated] makes no difference to the solution along this line. For numerical efficiency, it is desirable to choose an initial condition that leads to a multivariate solution that is smooth, or otherwise easy to represent. In our numerical methods, we set the initial condition to be a quasi-periodic solution of the circuit at $t_1 = 0$; the envelope solution then changes gradually as a function of t_1, and satisfactory efficiency is obtained.

C. Frequency-Modulated (FM) Signals

The efficiency of numerical methods relies on the multi-time representations admitting of a far more compact description than the traditional (single-time) form. While this is so for a large class of signals, such as those shown above, it is not universally true. Chaotic waveforms, for example, cannot be represented compactly in any known form. More importantly, from a practical standpoint, FM signals are not compact in the simple multivariate representations presented above; hence the numerical techniques presented in this paper are not useful for circuits with FM. In this section, we illustrate the problem; a solution is outlined elsewhere [4].

FM refers to a class of multirate signals in which the period of a rapidly-varying, locally-periodic waveform changes slowly. FM can be generated in forced oscillators such as voltage-controlled oscillators (VCOs), and is of great importance in communications. FM is qualitatively different from the multirate signals encountered so far in this paper, because unlike the examples in Figs. 3, 6 and 7, naïve multi-time representations of FM have many undulations are not easy to sample efficiently. We illustrate the difficulty using the following prototypical FM signal

$$
x(t) = \cos(\omega_2 t + k\cos(\omega_1 t)),
$$

where

$$
\omega_1 = \frac{2\pi}{T_1}, \quad \omega_2 = \frac{2\pi}{T_2}, \qquad T_1 \gg T_2. \qquad (8)
$$

A bivariate form can be defined as follows:

$$
\hat{x}(t_1, t_2) = \cos(\omega_2 t_2 + k\cos(\omega_1 t_1)),
$$

with

$$
x(t) = \hat{x}(t_1, t_2). \qquad (9)
$$

Note, that $\hat{x}$ is (T_1, T_2)-periodic, hence $x(t)$ is (T_1, T_2)-quasi-periodic.

$\hat{x}(t_1, t_2)$ is illustrated in Fig. 11. Note that if $k \gg 2\pi$, i.e., $k \approx 2\pi m$ for some large integer m, then $\hat{x}(t_1, t_2)$ will undergo about m oscillations as a function of t_1 over one period T_1. In practice, k is often of the order of $\omega_2 \gg 2\pi$, hence this number
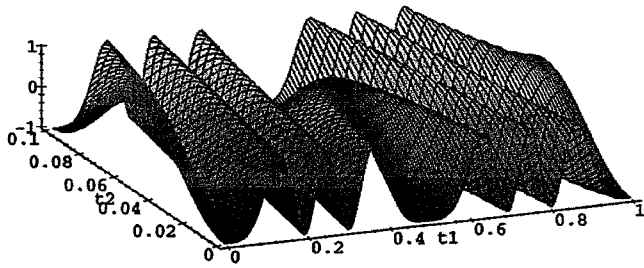
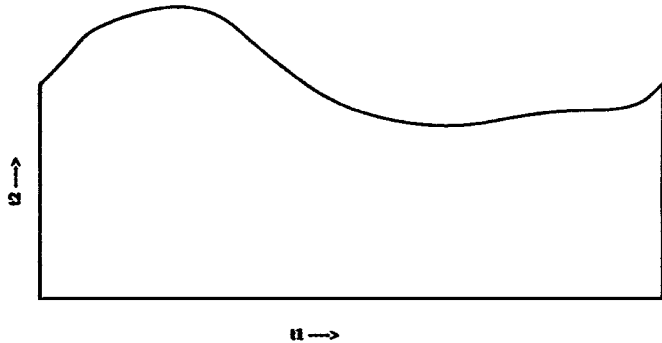Fig. 11. Bivariate representation of FM signal.

Fig. 12. Moving boundaries cannot generate steady-state solutions.

of oscillations can be very large. Therefore, it becomes difficult to represent $\hat{x}$ efficiently by sampling on a two-dimensional grid.

FM is usually thought of as a slow change in the frequency of a fast-varying signal. If the frequency of a periodic component is thought of as the inverse of the corresponding time-period, it is natural to hope that FM solutions can be captured by periodic solutions on nonrectangular regions with nonparallel boundaries. The concept is illustrated in Fig. 12, where the value of T_2 (the fast time-period) is no longer constant but varies along t_1. We now show, however, that the concept of varying time-period is not useful for capturing FM, by proving the fact that *nonparallel boundary edges cannot generate steady-state solutions*, i.e., neither the MPDE nor the underlying ODE can have quasi-periodic solutions derived from nonparallel boundaries.

For simplicity, assume a two-rate state-equation form for the MPDE of a forced oscillator

$$\frac{\partial \hat{x}}{\partial t_1} + \frac{\partial \hat{x}}{\partial t_2} = f(\hat{x}) + \hat{b}(t_1, t_2). \tag{10}$$

Assume that t_1 is the slow time scale, t_2 is the fast time scale, and that $\hat{b}$ is independent of t_2, as is reasonable for a forced oscillator. Now, assume that this system can be solved for periodic solutions on a moving boundary in the t_2 direction, given by the scalar function $T_2(t_1)$, which is T_1-periodic (see Fig. 12). This is equivalent to assuming the solution to be in the form

$$\hat{x}(t_1, t_2) = \hat{y}\left(\frac{t_1}{T_1}, \frac{t_2}{T_2(t_1)}\right), \qquad \hat{y} \text{ is } (1, 1)\text{-periodic.} \tag{11}$$

Now, expand the partial differentiation terms of (10) using (11)

$$\frac{\partial \hat{x}}{\partial t_1} = \frac{1}{T_1} \frac{\partial \hat{y}}{\partial a}\left(\frac{t_1}{T_1}, \frac{t_2}{T_2(t_1)}\right)$$

$$- \frac{\partial \hat{y}}{\partial b}\left(\frac{t_1}{T_1}, \frac{t_2}{T_2(t_1)}\right) \overbrace{\frac{t_2}{T_2^2(t_1)}}^{\text{secular term}} \frac{dT_2}{dt_1}(t_1) \tag{12}$$

$$\frac{\partial \hat{x}}{\partial t_2} = \frac{1}{T_2(t_1)} \frac{\partial \hat{y}}{\partial b}\left(\frac{t_1}{T_1}, \frac{t_2}{T_2(t_1)}\right). \tag{13}$$

Note, that (12) contains a so-called *secular term* [5], i.e., a term that increases linearly with t_2 if $T_2(t_1)$ is not a constant. Note further that all other terms of (10) are of the form of (11), i.e., periodic, whereas the secular term increases unboundedly with t_2. Therefore, no solution of the form of (11) can exist, unless $T_2(t_1)$ is independent of t_1 (i.e., rectangular boundaries). A similar argument can be used to establish that even the DAE of the forced oscillator cannot admit solutions of the type $\hat{x}(t, t)$, with $\hat{x}$ in the form (11). This conclusion is also physically reasonable, for the secular term would imply that the instantaneous frequency of the signal grows unboundedly, which is unphysical.

Despite the negative result above, FM signals can in fact be represented compactly with multiple times, leading to efficient methods for solving forced oscillators [4].

V. NUMERICAL SOLUTION OF THE MPDE

In this section, four numerical methods are presented for solving the MPDE. Three of the methods [multivariate FDTD (MFDTD), hierarchical shooting (HS), and time-domain envelope (TD-ENV)] are set purely in the time domain. The multivariate mixed frequency-time (MMFT) method is used to solve for some of the dimensions of the MPDE in the frequency domain and others in the time domain.

The purely time domain methods presented here are suitable for signals whose every component is influenced by strong nonlinearities. If some signal paths are mildly nonlinear while others are strongly nonlinear, as is the case in some types of communication circuits (e.g., switching mixers, switched-capacitor circuits), the mixed frequency-time method can be more efficient because it uses a short Fourier series for the mildly nonlinear components. For efficient sampling of the multivariate waveforms, adaptively generated nonuniform grids can be used.

A. The MFDTD Method

In this method, the MPDE (6) is solved on a grid in the $t_1, \ldots, t_m$ space. Let the grid be the set of points $\{\bar{t}_1, \ldots, \bar{t}_n\}$, where each $\bar{t}_i = (t_{1_i}, \ldots, t_{m_i})$. The partial differentiation operators of the MPDE are discretized and the MPDE collocated on this grid. This leads to a set of nonlinear algebraic equations in the unknowns $\{\hat{x}(\bar{t}_1), ., \hat{x}(\bar{t}_n)\}$. The nonlinear equations are solved by numerically, using, e.g., Newton–Raphson or continuation methods.

For concreteness, consider the two-rate case. The MPDE simplifies to

$$\frac{\partial q(\hat{x})}{\partial t_1} + \frac{\partial q(\hat{x})}{\partial t_2} = f(\hat{x}) + \hat{b}(t_1, t_2) \tag{14}$$

with periodic BCs $\hat{x}(t_1 + T_1, t_2 + T_2) = \hat{x}(t_1, t_2)$. Consider a uniform grid $\{\bar{t}_{i,j}\}$ of size $n_1 \times n_2$ on the rectangle $[0, T_1] \times [0, T_2]$. Here $\bar{t}_{i,j} = (t_{1_i}, t_{2_j})$, $t_{1_i} = (i-1)h_1$ and $t_{2_j} = (j-1)h_2$, $1 \le i \le n_1$, $1 \le j \le n_2$. $h_1 = T_1/n_1$ and $h_2 = T_2/n_2$ are the grid spacings in the t_1 and t_2 directions respectively.

Discretizing the differentiation operators using (for example) the Backward Euler rule leads to

$$\frac{\partial q(\hat{x})}{\partial t_1}(\bar{t}_{i,j}) = \frac{q(\hat{x}(\bar{t}_{i,j})) - q(\hat{x}(\bar{t}_{i-1,j}))}{h_1}$$

$$\frac{\partial q(\hat{x})}{\partial t_2}(\bar{t}_{i,j}) = \frac{q(\hat{x}(\bar{t}_{i,j})) - q(\hat{x}(\bar{t}_{i,j-1}))}{h_2}. \tag{15}$$

Collocating the MPDE at the grid points $\{\bar{t}_{i,j}\}$ leads to $n = n_1 \times n_2$ equations

$$F_{i,j} \equiv \frac{\hat{q}_{i,j} - \hat{q}_{i-1,j}}{h_1} + \frac{\hat{q}_{i,j} - \hat{q}_{i,j-1}}{h_2} - \hat{f}_{i,j} - b_{i,j} = 0$$

$$\forall i \in \{1, \ldots, n_1\} \quad \forall j \in \{1, \ldots, n_2\}$$

$$\hat{q}_{i,j} = q(\hat{x}(\bar{t}_{i,j})), \quad \hat{f}_{i,j} = f(\hat{x}(\bar{t}_{i,j})) \quad \hat{b}_{i,j} = \hat{b}(\bar{t}_{i,j}). \tag{16}$$

The n equations are, however, in a greater number of unknowns; $n_1 + n_2$ extra unknowns $\{\hat{x}(\bar{t}_{-1,j})\}$ and $\{\hat{x}(\bar{t}_{i,-1})\}$ result from discretizing the differentiation operators on the $t_1 = 0$ and $t_2 = 0$ lines respectively. These unknowns are eliminated using the biperiodic BCs of the MPDE

$$\hat{x}(\bar{t}_{i,-1}) = \hat{x}(\bar{t}_{i,n_2-1}) \qquad \hat{x}(\bar{t}_{-1,j}) = \hat{x}(\bar{t}_{n_1-1,j}). \tag{17}$$

On applying the BCs, $n_1 + n_2$ unknowns are eliminated from (16) and a system of n equations in n unknowns is obtained. Denote this system by

$$F(X) = 0$$

where

$$F = [F_{1,1}, \ldots, F_{1,n_2}, F_{2,1}, \ldots, F_{n_1,1}, \ldots, F_{n_1,n_2}]^T$$

$$X = [\hat{x}(\bar{t}_{1,1}), \ldots, \hat{x}(\bar{t}_{1,n_2}), \hat{x}(\bar{t}_{2,1}), \ldots, \hat{x}(\bar{t}_{n_1,n_2})]^T. \tag{18}$$

Equation (18) can now be solved numerically by any numerical method for nonlinear equation systems, e.g., Newton–Raphson or continuation [17]. Typically, nonlinear solution algorithms require the repeated solution of linear systems involving the Jacobian matrix of $F(\cdot)$. This Jacobian has the block structure

$$\frac{\partial F}{\partial X} = \begin{bmatrix} D_1 + L_1 & & & & -L_{n_1} \\ -L_1 & D_2 + L_2 & & & \\ & -L_2 & & & \\ & & & \ddots & \\ & & & -L_{n_1-1} & D_{n_1} + L_{n_1}. \end{bmatrix} \tag{19}$$

Each block is itself a $n_2 \times n_2$ block-matrix, given by (20) and (21), shown at the bottom of the page. In (19), $q'_{i,j} = q'(\hat{x}(\bar{t}_{i,j}))$ and $f'_{i,j} = f'(\hat{x}(\bar{t}_{i,j}))$.

In the above, a uniform grid was assumed for simplicity. In practice, the grid is nonuniform, built by starting from a coarse grid and adapting to the shape of the waveforms for higher accuracy and efficiency.

$\partial F/\partial X$ is evidently a sparse matrix, hence matrix-vector products with it can be performed cheaply. This makes iterative linear techniques (e.g., [18], [11], [9], [19]) attractive for solving linear systems involving the Jacobian. In this context,

$$D_i = \begin{bmatrix} \left(\dfrac{q'_{i,1}}{h_2} + f'_{i,1}\right) & & & & & -\dfrac{q'_{i,n_2}}{h_2} \\ -\dfrac{q'_{i,1}}{h_2} & \left(\dfrac{q'_{i,2}}{h_2} + f'_{i,2}\right) & & & & \\ & -\dfrac{q'_{i,2}}{h_2} & & & & \\ & & \ddots & & & \\ & & & -\dfrac{q'_{i,n_2-1}}{h_2} & \left(\dfrac{q'_{i,n_2}}{h_2} + f'_{i,n_2}\right) \end{bmatrix} \tag{20}$$

$$L_i = \frac{1}{h_1} \begin{bmatrix} q'_{i,1} & & & & \\ & q'_{i,2} & & & \\ & & q'_{i,3} & & \\ & & & \ddots & \\ & & & & q'_{i,n_2} \end{bmatrix} \tag{21}$$

diagonal dominance characteristics of the Jacobian are useful for effective preconditioning. For uniform gridding of the scalar case, with q linear, the Jacobian is diagonally dominant if f' has the same sign as q', as is the case for stable circuits. When f and q are vector functions, block-diagonal dominance (under the Frobenius norm) holds for linear $q(\cdot)$ and uniform grids. Even in circuits with nonlinear $q(\cdot)$ and nonuniform grids for capturing highly nonlinear behavior, diagonal and lower triangular preconditioners are much more effective than for harmonic balance, in which diagonal dominance is lost as the nonlinearities grow stronger.

B. HS

The two commonly used methods for finding periodic steady states of one-tone circuits are shooting and harmonic balance. In a sense, the two methods are symmetric, operating in dual domains with complementary advantages and disadvantages. Yet there remains an asymmetry between them: while HB is easily extended to more than one tone, the same is not true of shooting. This imbalance can be redressed in a natural manner using the MPDE formulation, which permits a hierarchical extension of the classical shooting algorithm for multiple tones. In this section, this scheme, which we call Hierarchical Shooting (HS), is outlined.

The key to this method is to view the MPDE as an ordinary differential equation in *function space* variables. For concreteness, consider again the two-time MPDE of (14)

$$\frac{\partial q(\hat{x})}{\partial t_1} + \frac{\partial q(\hat{x})}{\partial t_2} = f(\hat{x}) + \hat{b}(t_1, t_2). \qquad (22)$$

In (22), the variables $\hat{x}$, q, f and $\hat{b}$ are all vector-valued functions of two variables t_1 and t_2, i.e., they are maps from $\mathcal{R}^2 \mapsto \mathcal{R}^k$, where k is the size of the circuit. However, they can each be also regarded as functions of a *single* variable with values that are vector-valued *functions*, i.e., they are maps from $\mathcal{R} \mapsto \{h(\cdot): \mathcal{R} \mapsto \mathcal{R}^k\}$. Let $Q(t_1)$, $X(t_1)$, $F(t_1)$ and $B(t_1)$ be functions of t_1, with values that are functions (of t_2), i.e., $q(t_1, t_2)$, $\hat{x}(t_1, t_2)$, $f(t_1, t_2)$ and $\hat{b}(t_1, t_2)$ respectively (the function-valued variables F and X should not be confused with the vector-valued ones of the previous section). In other words, the value of, e.g., $Q(t_1)$, for a fixed t_1, equals the *entire function* $q(t_1, \cdot)$.

The MPDE can then be written formally as a DAE in function-valued variables, using operator notation

$$\frac{dQ(X)}{dt_1} = F(X) + B(t_1) - \mathcal{D}_{t_2}[Q(X)] \qquad (23)$$

$\mathcal{D}_{t_2}$ is an operator that differentiates the function (of t_2) that it operates on.

The methodology of shooting can now be applied to (23). Let $\Phi(X_0, t)$ be the "state-transition function" of the DAE, i.e., the response of (23) at time t to an initial condition function $X_0 = X(0)$ imposed at $t_1 = 0$. Shooting consists of solving the equation

$$\Phi(X, T_1) - X = 0 \qquad (24)$$

using (for example) the Newton–Raphson method. In classical shooting, the Jacobian of the equation corresponding to (23) is a matrix. The Jacobian of (24), however, is not a simple matrix; rather, it is a linear operator on the space of vector-valued functions of t_2. Further, each evaluation of the left-hand-side of (24) involves an initial-value solution of (23). This is performed by discretizing (23) using (for example) Backward Euler

$$\frac{Q(X(t_{1_i})) - Q(X(t_{1_{i-1}}))}{t_{1_i} - t_{1_{i-1}}}$$
$$= F(X(t_{1_i})) + B(t_{1_i}) - \mathcal{D}_{t_2}[Q(X(t_{1_i}))] \qquad (25)$$

and solving for the unknown $X(t_{1_i})$ (i.e., X at the current time-point i). Note, that (25) is itself a differential equation in t_2, since it can be rewritten as

$$\frac{dQ(X(t_{1_i}))}{dt_2} = -\frac{Q(X(t_{1_i})) - Q(X(t_{1_{i-1}}))}{t_{1_i} - t_{1_{i-1}}}$$
$$+ F(X(t_{1_i})) + B(t_{1_i}). \qquad (26)$$

Equation (26) can be solved using shooting (or another method, e.g., univariate FDTD or harmonic balance) in t_2, but in a lower dimension. This "inner loop" solution is performed for each time-step in the t_1 dimension of the "outer loop" of (23).

An advantage of hierarchical shooting over multivariate FDTD is that the size of the linear systems that need to be solved is smaller, by the number of points in the t_1 dimension. In other words, whereas the size of the Jacobian matrix for multivariate FDTD was $kn_1 n_2$ (k = circuit size), that for hierarchical shooting is kn_2. This leads to memory savings, but can also lead to more computation compared to MFDTD, depending on how many shooting iterations are needed. Circuits with slowly dying oscillations (e.g., high-Q circuits) often require many shooting iterations. The grid in hierarchical shooting is induced naturally by the time-step control of the transient analysis algorithm, and explicit gridding algorithms are not needed.

C. The TD-ENV Method

The initial-value solutions encountered in HS, i.e., (23), are useful in their own right for envelope following. Given an initial condition function specified at $t_1 = 0$, (23) can be solved without searching for a periodic solution, i.e., (24) need not be enforced. On discretization, (25) results, which is solved for a periodic solution in t_2 using (26). Any method can be used for this inner loop; in particular, for strongly nonlinear problems, time-domain methods like shooting or FDTD can be used. This constitutes a purely time-domain algorithm for multi-tone envelope following.

D. The MMFT Method

Since $\hat{x}(t_1, \ldots, t_m)$ and $\hat{b}(t_1, \ldots, t_m)$ are m-periodic, they can be expressed as Fourier series in each variable t_i. If the circuit is such that some of the variables have relatively few significant Fourier components (as in, e.g., switched-capacitor filters and switching mixers), then it can be more efficient to solve the
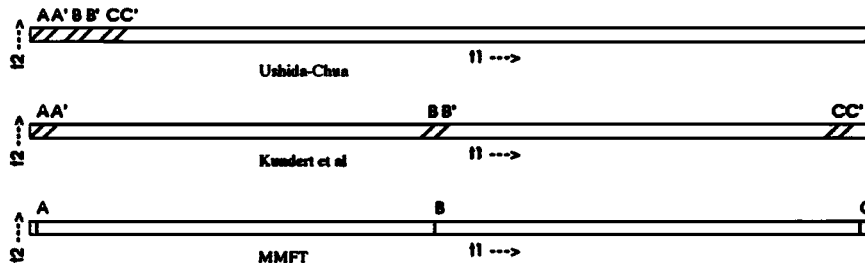
Fig. 13. Different MFT methods.

mixed frequency-time system obtained by taking a Fourier series expansion of the MPDE in those variables. The two-time case is used again for exposition. Equation (14) is rewritten as a Fourier series in t_1:

$$
\sum_{i=-M}^{M} ij\omega_1 Q_i(t_2)e^{ij\omega_1 t_1} + \sum_{i=-M}^{M} \frac{\partial Q_i(t_2)}{\partial t_2} e^{ij\omega_1 t_1}
$$
$$
= \sum_{i=-M}^{M} F_i(t_2)e^{ij\omega_1 t_1} + \sum_{i=-M}^{M} B_i(t_2)e^{ij\omega_1 t_1} \quad (27)
$$

where

$j \qquad = \sqrt{-1};$
$\omega_1 \qquad = 2\pi/T_1;$
Q_i, F_i, B_i Fourier components in t_1 of $q(\hat{x}(t_1, t_2))$, $f(\hat{x}(t_1, t_2))$ and $\hat{b}(t_1, t_2)$, respectively;
$M \qquad$ (small) number of significant harmonics.

Since the functions $e^{ij\omega_1 t_1}$ are linearly independent, the Fourier components in (27) can be equated

$$
ij\omega_1 Q_i(t_2) + \frac{\partial Q_i(t_2)}{\partial t_2} = F_i(t_2) + B_i(t_2),
$$
$$
i \in \{-M, \dots, M\} \quad (28)
$$

(28) can be rewritten in vector form

$$
\frac{d\overline{Q}(t_2)}{dt_2} = -j\Omega_1 \overline{Q}(t_2) + \overline{F}(t_2) + \overline{B}(t_2) \quad (29)
$$

where

$$
\Omega_1 = \omega_1 \begin{bmatrix} M & & & & \\ & \ddots & & & \\ & & 0 & & \\ & & & \ddots & \\ & & & & -M \end{bmatrix}
$$

$$
\overline{Q} = \begin{bmatrix} Q_M \\ \vdots \\ Q_0 \\ \vdots \\ Q_{-M} \end{bmatrix}, \quad \overline{F} = \begin{bmatrix} F_M \\ \vdots \\ F_0 \\ \vdots \\ F_{-M} \end{bmatrix}, \quad \overline{B} = \begin{bmatrix} B_M \\ \vdots \\ B_0 \\ \vdots \\ B_{-M} \end{bmatrix}.
$$
$$(30)$$

Equation (29), being a vector DAE, is solved for a periodic solution by existing time-domain methods such as univariate

shooting [20], [21] or univariate FDTD. Solution in the time domain makes it possible to use nonuniform time-steps and hence to capture the effects of strong nonlinearities efficiently. The differentiation operator is discretized using a numerical integration scheme. This results in an inner system of frequency-domain equations that are solved by harmonic balance. An alternative method using shooting/FDTD in the inner loop and harmonic balance in the outer can also be derived, using the function-space variable concept of Section V-B.

E. Unifying Aspects of the MPDE

A pleasing feature of the MPDE is that, in addition to generating the new methods above, it also provides a framework for unifying previous methods for solving multirate circuits. Multi-tone harmonic balance has already been shown to be the result of expressing the MPDE in multidimensional Fourier series [7]. Previous envelope methods are also easily derived from the MPDE. For example, (29) can be solved as an initial value problem rather than with periodic BCs. This results in a simpler derivation of our previous envelope-following method based on HB [13], with the further advantage that restrictions on the relative time-scales of the tones are removed.

The time-frequency methods of Ushida and Chua [14] and Kundert et al. [15] are also easily visualized using the MPDE on two time scales. Consider one of the t_1–t_2 rectangles shown in Fig. 13, with t_1 the direction of the slower time scale. These methods rely on a Fourier series assumption along the t_1 axis to generate constraints between points separated by one period of the fast time scale. For example, assume that the variation of the solution along the upper edge of the t_1–t_2 rectangle is captured by a Fourier series with a dc term and one harmonic, i.e., a total of 3 real numbers. Then, these Fourier coefficients are uniquely determined by sampling three points, e.g., the set A, B and C, or the set A′, B′ and C′ in Fig. 13. This leads to three equations relating the six samples. Three more equations, relating pairs of samples at (A, A′), (B, B′) and (C, C′), result from the DAE. By solving the equations together, all six samples can be determined.

An important difference between MMFT and the methods of Ushida/Chua and Kundert et al. is in the choice of the points A, A′, B, B′, C, C′, as shown in Fig. 13. The latter two methods are constrained by the requirement that pairs of points be separated by one period of the fast time-scale. This corresponds to nonoptimal sampling along the slow time scale, leading to numerical ill-conditioning. In the limit, as the ratio of the t_1 period to the t_2 period tends to infinity, the equation system grows singular. This problem is avoided by the MMFT method, which corre-

TABLE I
CPU TIMES (SPARC 20, 96 MB, SunOS4.1.3)

Circuit	New method	Univariate shooting	Speedup
rectifier, MFDTD	40s	1h 21m	121.5
rectifier, HS	1m 09s	1h 36m	83.47
mixer, MMFT	25s	1h 52m	250.8

Fig. 14. Pulse$(t, 0.3)$.

sponds to using perfectly conditioned, uniform samples along the t_1 axis and enforcing exact equality conditions between the ends of vertical lines.

VI. SAMPLE APPLICATIONS

In this section, the methods of the previous sections are applied to power converters, switched-capacitor circuits and switching mixers. The circuits and waveforms are described in the following sections. Some CPU times from the new methods are compared against those from previous methods in Table I.

Speedups of two orders of magnitude are obtained using the new methods. In addition, while univariate shooting for multirate problems tends to accumulate errors that can lead to gross inaccuracies, the new methods maintain accuracy maintain accuracy.

A. Rectifier, Quasi-Periodic Simulation with MFDTD

A diode rectifier circuit, powered by a large quasi-periodic two-tone power source $b(t)$, was simulated for a quasi-periodic solution using MFDTD. The circuit consisted of a diode followed by a parallel *RC* filter combination. The power source was a train of fast pulses whose duty cycle was modulated at a much slower rate. Using pulse $(t/0.1\,\mu, \text{duty})$ to describe each pulse (shown in Fig. 14 for a duty cycle of 0.3), the excitation $b(t)$ was

$$b(t) = \text{pulse}\left(\frac{t}{T_2}, 0.2 + 0.3\sin\left(\frac{2\pi t}{T_1}\right)\right),$$
$$T_1 = 1\,\text{ms} \quad T_2 = 0.1\,\mu\text{s}.$$

Two segments of $b(t)$, at widely separated times, are plotted in Fig. 15, illustrating the variation in duty cycle. The duty-cycle variation of $b(t)$ is more apparent in its bivariate form $\hat{b}(t_1, t_2)$:

$$\hat{b}(t_1, t_2) = \text{pulse}\left(\frac{t_2}{T_2}, 0.2 + 0.3\sin\left(\frac{2\pi t_1}{T_1}\right)\right),$$
$$T_1 = 1\,\text{ms} \quad T_2 = 0.1\,\mu\text{s}$$

$\hat{b}(t_1, t_2)$ form is plotted in Fig. 16. The duty cycle is the extent of the high region while moving along the t_2 direction, varying sinusoidally with respect to the slow variable t_1.

The bivariate form $\hat{x}$ of the output $x(t)$ is shown in Fig. 17. The low-pass filter has smoothed out the fast variations in the t_2 direction. Since the rectified output depends on the duty cycle on the input, a slow-scale sinusoidal variation is observed as a function of t_1. The circuit was also simulated by univariate shooting for comparison. As shown in Table I, the MFDTD method was faster by over two orders of magnitude. Plots of the univariate
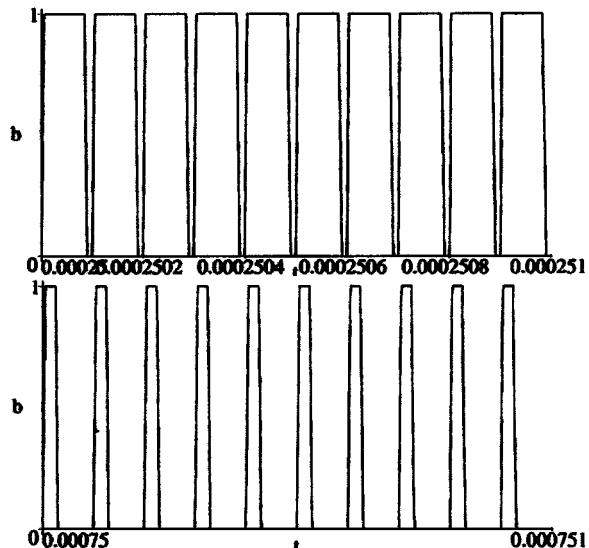
Fig. 15. $b(t)$: detail at widely separated times.
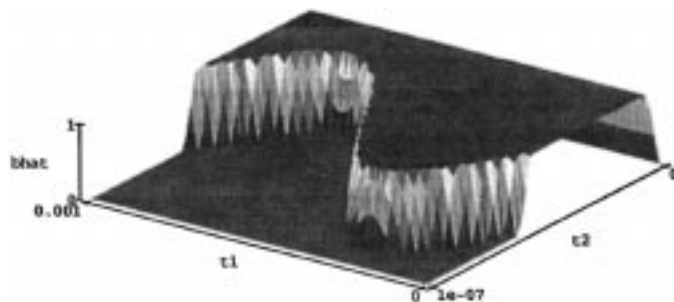
Fig. 16. The bivariate excitation $\hat{b}(t_1, t_2)$.
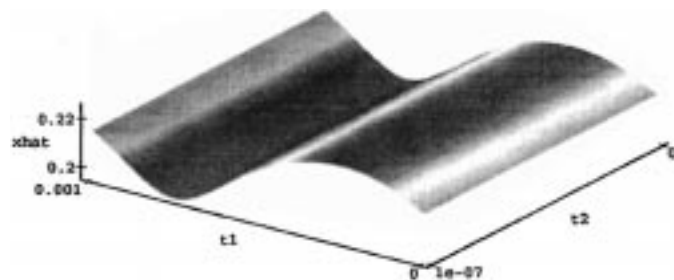
Fig. 17. The bivariate solution $\hat{x}(t_1, t_2)$.

solution $x(t)$ are shown in Fig. 18. The waveform obtained by setting $t_1 = t_2 = t$ in the bivariate solution is denoted by the legend "new," and those from univariate shooting using 20 and
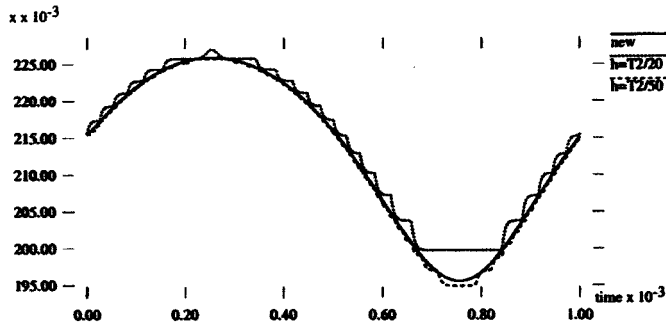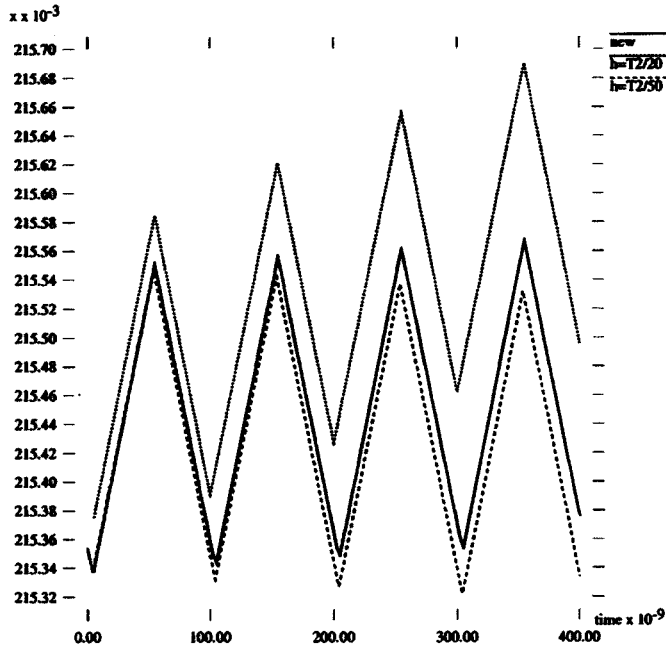
Fig. 18.   Rectifier $x(t)$ slow-scale variation.

Fig. 19.   Rectifier output fast-scale variation.

50 time-steps per fast pulse by "$h = T2/20$" and "$h = T2/50$" respectively. Univariate shooting using 20 time-steps per pulse accumulated errors that grew to 15% near $t = 0.8$ ms, despite tight local error control. Increasing the number of time-steps to 50 per pulse reduced the error, but it remained significant at about 3% (the CPU time in Table I is for this simulation). MFDTD produced the correct waveform.

The fast-scale detail of $x(t)$ near $t = 0$ is shown in Fig. 19. Because of the relatively long time-constant of the smoothing RC filter, the shape of the ripple is nearly triangular.

B. Rectifier, Envelope Simulation with TD-ENV

The rectifier circuit of the previous simulation, but with a more abrupt excitation, was simulated for an envelope waveform using TD-ENV. In this simulation, the duty cycle of the excitation switched abruptly between 0.2 and 0.8, instead of varying slowly as a sinusoid. $b(t)$ was given by

$$b(t) = \text{pulse}\left(\frac{t}{T_2}, 0.2 + 0.6\,\text{pulse}\left(\frac{t}{T_1}\right)\right),$$

$$T_1 = 1\,\text{ms} \quad T_2 = 0.1\,\mu\text{s}.$$

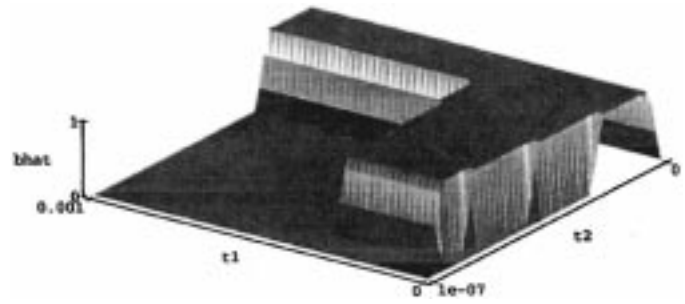The bivariate form $\hat{b}(t_1, t_2)$ is shown in Fig. 20.
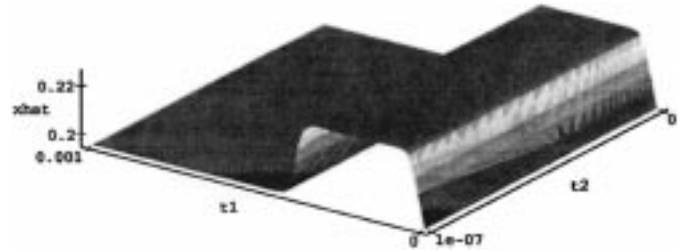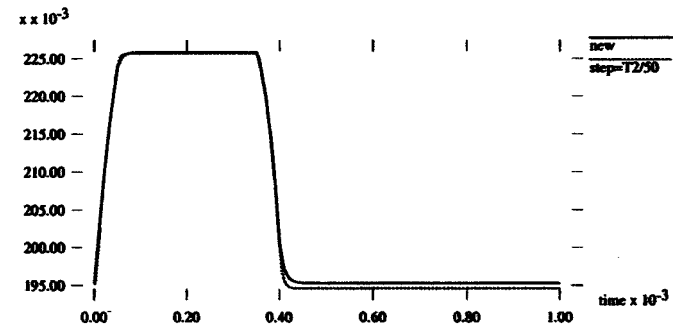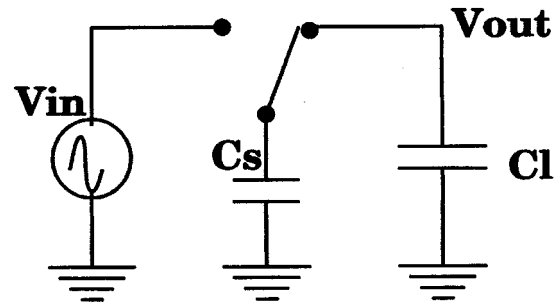

Fig. 20. $\hat{b}(t_1, t_2)$: pulse in both variables.

Fig. 21. $\hat{x}(t_1, t_2)$ for abrupt slow-scale excitation.

Fig. 22. $x(t)$ for abrupt slow-scale excitation.

The bivariate form $\hat{x}$ of the output is shown in Fig. 21. The variation in t_2 has been smoothed out as before, but the variation in t_1 now resembles a pulse, as expected.

The univariate solution is plotted in Fig. 22. A 3% inaccuracy from univariate shooting with 50 steps per fast pulse is again evident.

C. Switched-Capacitor Filter with MFDTD

MFDTD was used to simulate a one-pole switched-capacitor filter, depicted in Fig. 23. If the switching is much faster than the variation of the input signal, then the switch and C_s act like
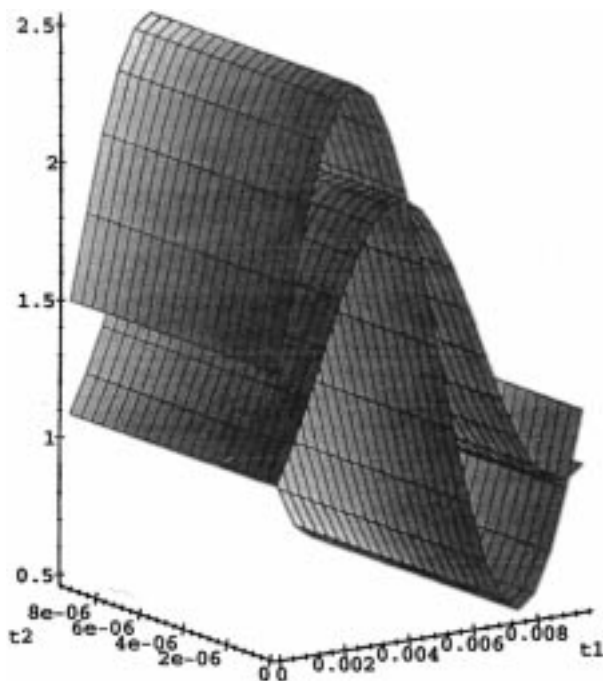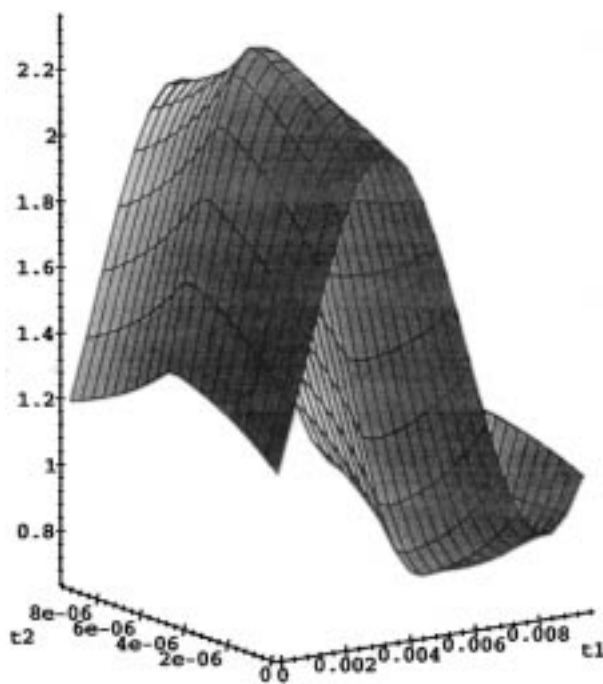

Fig. 23.   Switched capacitor filter.

Fig. 24. SC filter input and output.

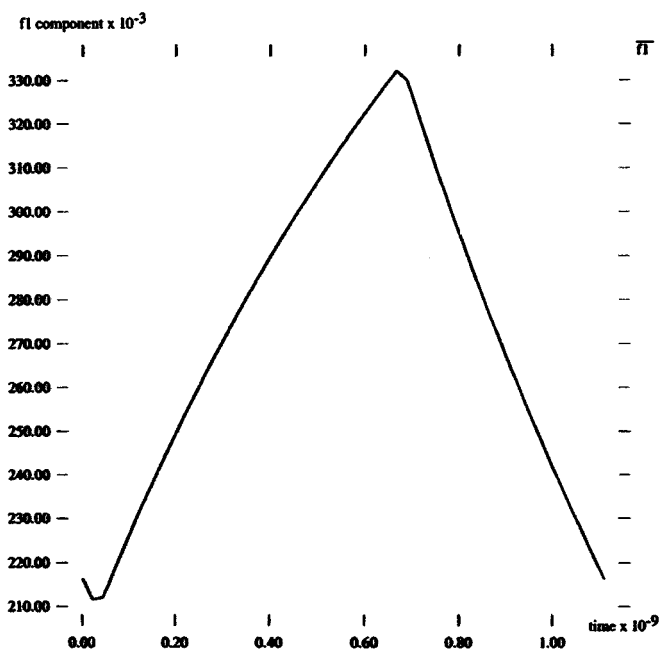Fig. 25. SC filter input and output.

Fig. 26. Mixed frequency-time output: first harmonic component.

variation along the slow time scale is apparent; note the absence of fast-time-scale variation at the output, indicating that the switching frequency has been eliminated by filtering (the input, by definition, has no fast variation). Note, also the phase shift of the output with respect to the input. In contrast to the filtered output, the switches exhibit strong fast scale variation, since rapid switching is key to the proper operation of the circuit. The bivariate form of the voltage at the one of the switch capacitors is shown in Fig. 25. Note the variation along both slow and fast time-scales. The slow time-scale variation is similar to the input, as expected, but the fast time-scale variation displays charging/discharging behavior associated with internal losses in the switch, due to the relatively fast switching speed.

The second harmonic distortion, obtained by Fourier analysis of the output voltage along the t_1 direction, was 28 dB below the fundmental.

D. Mixer Simulation Using MMFT

A double-balanced switching mixer and filter circuit was simulated for intermodulation distortion using the MMFT method. The RF input to the mixer was a 100 kHz sinusoid with amplitude 100 mV; this sent it into a mildly nonlinear regime. The LO input was a square wave of large amplitude (1 V), which switched the mixer on and off at a fast rate (900 MHz).

Three harmonics were taken in the RF tone $f_1 =$ 100 kHz (corresponding to the t_1 variable of Section V-D). The LO tone at $f_2 =$ 900 MHz was handled by shooting in the t_1 variable. The output of the algorithm is a set of time-varying harmonics that are periodic with period $T_2 = 1/f_2$. The first harmonic is shown in Fig. 26. This plot contains information about all mix components of the form $f_1 + if_2$, i.e., the frequencies 900.1 MHz, 1800.1 MHz, etc. The main mix component of interest, 900.1 MHz, is found by taking the first Fourier component of the waveform in Fig. 26. This has an amplitude of 60 mV.

a resistor, which, together with the capacitor C_l, constitute the filter. The effective value of the switched-capacitor resistor is T_2/C_r, where T_2 is the period of the switch control. The values of the switch capacitance C_s and filter capacitor C_l were 50 nF and 5 μF, respectively.

The input to the circuit was a sinusoid with 10 ms period (100 Hz), and the switching period was 10^{-5} s (100 kHz). The slow time scale was taken to be t_1, and the fast time-scale was t_2. Bivariate forms of the input and output voltages are both shown in Fig. 24 (the larger waveform is the input). The
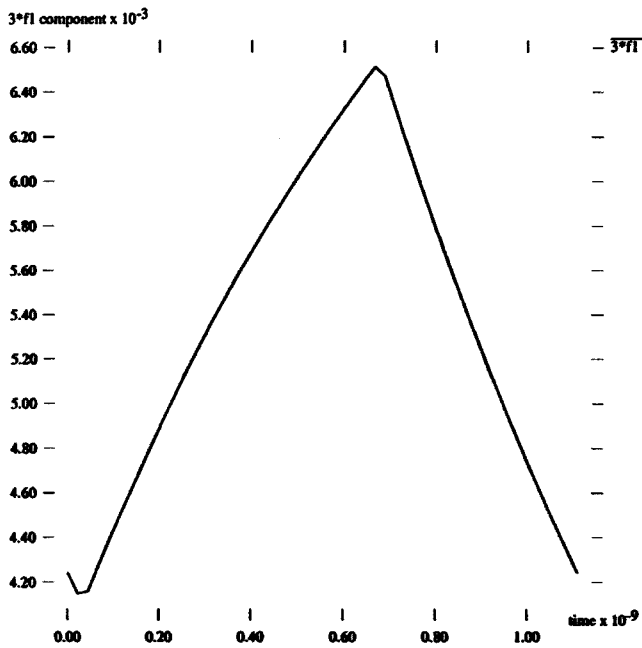
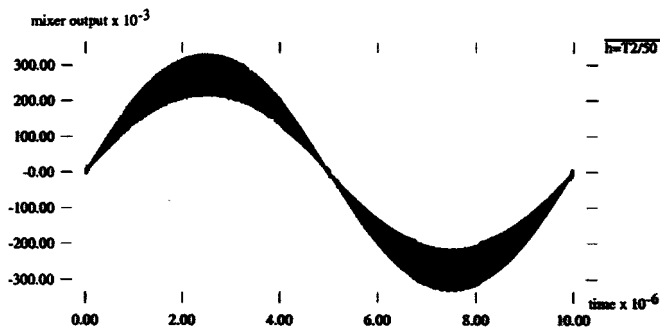Fig. 27.   Mixed frequency-time output: third harmonic component.
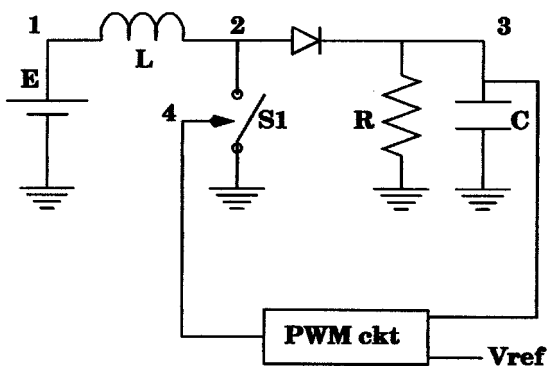

Fig. 28.   Mixer output from univariate shooting.

Fig. 29.   PWM DC–DC converter.

The third harmonic is shown in Fig. 27. It contains information about the mixes $3f_1 + if_2$, i.e., the frequencies 900.3 MHz, 1800.3 MHz, etc. The amplitude of the 900.3 MHz component can be seen to be about 1.1 mV. Hence, the distortion introduced by the mixer is about 35 dB below the desired signal.

The circuit was also simulated by univariate shooting for comparison. The output from univariate shooting is shown in Fig. 28. This run, using 50 steps per fast period, took almost 300 times as long as the new algorithm (see Table I).
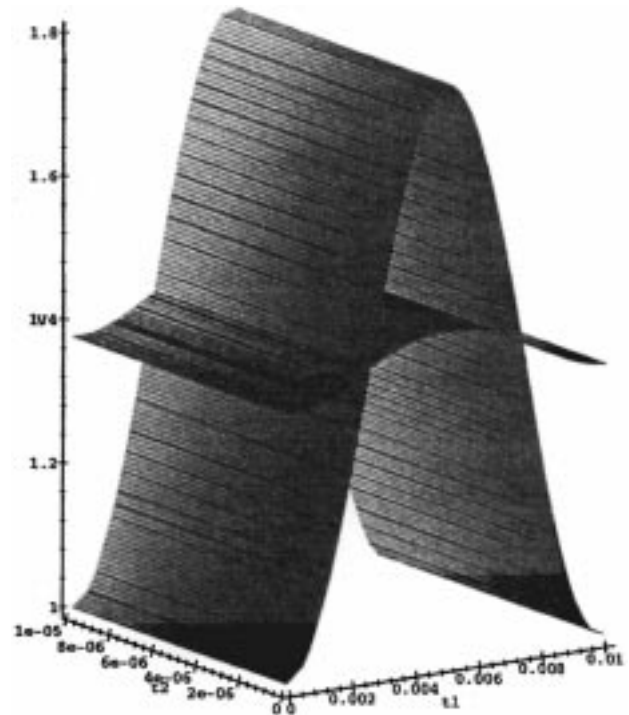

Fig. 30.   PWM DC–DC converter: input and output voltages.

E. PWM-Feedback DC–DC Converter with TD-ENV

A boost-type dc–dc converter with PWM feedback for output voltage stabilization was simulated by TD-ENV. A simplified diagram of the circuit is shown in Fig. 29. When the switch closes, the inductor current rises linearly until the switch opens, after which the current is diverted through the diode into the load resistor. The peak current of the inductor is related to the amount of time the switch is closed, i.e., the duty cycle of the switch control. This current determines the output voltage at node 3.

The negative feedback loop operates by comparing the output voltage at node 3 with a reference to obtain an error voltage, which is used to control the duty cycle of the control to the switch. If the output voltage is lower than the reference, the duty cycle is increased, and vice-versa. For the simulation, the input power source E was centered at 1.4 V, but with a ripple of 0.8 V at 100 Hz added. The reference voltage for the output was also set at 1.4V. The switching rate was 100 kHz. The bivariate forms of the input and output voltages are shown in Fig. 30; the large changes are for the input waveform, and the small ones for the regulated output. Note the relative absence of fast scale variation (i.e., along the t_2 axis) of the output, indicating low ripple. The current through the inductor is shown in Fig. 32. This waveform provides a useful visualization of the operation of the converter. Note the linear charging of the inductor and the somewhat nonlinear discharge. Note also that the converter is operating in continuous mode, for the current does not ever reach zero despite the fluctuations of the source battery. When the load is increased (not pictured), the inductor discharges completely for part of the fast time scale.

The dynamics of the feedback mechanism are also evident in the shape of the control voltage to the switch, shown in Fig. 31. This voltage is a fast pulse train with varying duty cycle. The
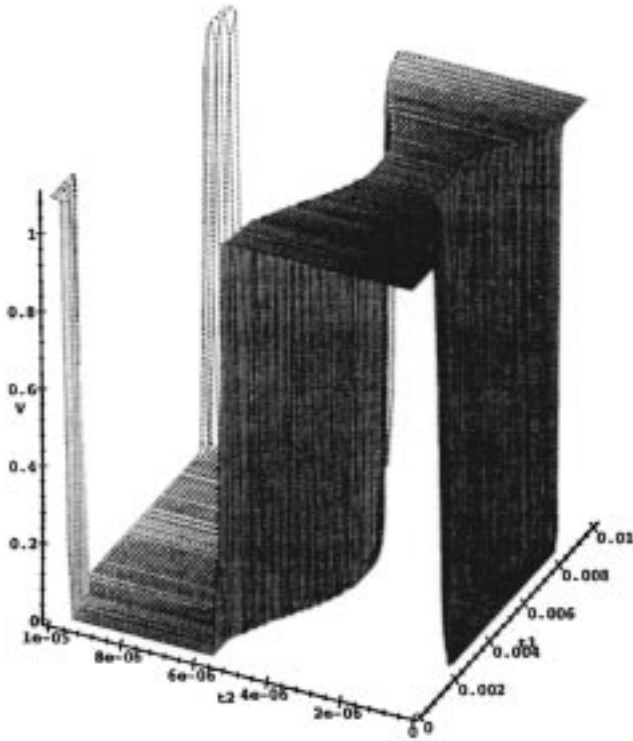
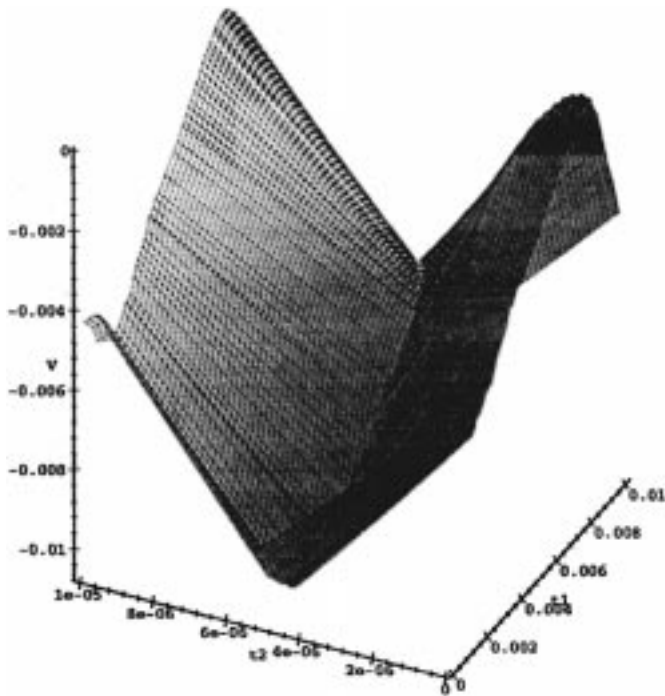Fig. 31.   PWM dc–dc converter: switch control.

Fig. 32.   PWM dc–dc converter: inductor current.

pulse nature of the signal is evident from the variation in the t_2 direction. The change of the duty cycle along the slow time scale can also be readily seen. This is due to feedback, which modifies the pulse width to keep the output voltage stable despite large input fluctuations.

VII. Conclusion

A powerful approach for analyzing strongly nonlinear multirate circuits has been presented. The approach uses multiple time variables to describe multirate behavior, leading to a PDE called the MPDE. Applying appropriate BCs to the MPDE leads to quasi-periodic and envelope-modulated solutions. Efficiency is achieved without compromising accuracy by using adaptive time-domain numerical techniques to solve the MPDE numerically. Three purely time-domain methods resulting from the approach are useful for strongly nonlinear circuits in general, while a fourth mixed frequency-time method is especially suitable for circuits with a mix of strong and weak nonlinearities. The new techniques can solve a variety of circuits that are hard to simulate with previous techniques. Presenting the results in three-dimensional form is useful for visualizing waveforms with widely separated time scales. Applications to switched-capacitor filters, switching mixers and power converters have been presented.

Appendix
Proofs of Theorems and Lemmas

Proof of Theorem 1 (MPDE-DAE Relation): Since

$$q(x(t)) = q(\hat{x}(t + c_1, \ldots, t + c_m)),$$

$$\frac{\partial q(x(t))}{\partial t} = \frac{\partial q(\hat{x}(t + c_1, \ldots, t + c_m))}{\partial t_1} + \cdots$$

$$+ \frac{\partial q(\hat{x}(t + c_1, \ldots, t + c_m))}{\partial t_m}$$

$$= f(\hat{x}(t + c_1, \ldots, t + c_m))$$
$$+ \hat{b}(t + c_1, \ldots, t + c_m) \text{ [by (6)]}$$

$$= f(x(t)) + b(t).$$
∎

Proof of Lemma 1: Being m-periodic, $\hat{y}(t_1, \ldots, t_m)$ can be expanded in a multidimensional Fourier series

$$\hat{y}(t_1, \ldots, t_m) = \sum_{i_1, \ldots, i_m} Y(i_1, \ldots, i_m)$$

$$\cdot \exp\left(j 2\pi \left(\frac{i_1 t_1}{T_1} + \cdots + \frac{i_m t_m}{T_m}\right)\right).$$

$y(t)$ is obtained in quasi-periodic form by substituting $t_i = t + c_i$

$$y(t) = \sum_{i_1, \ldots, i_m} \left[Y(i_1, \ldots, i_m) \right.$$

$$\cdot \exp\left(j 2\pi \left(\frac{i_1 c_1}{T_1} + \cdots + \frac{i_m c_m}{T_m}\right)\right)\Bigg]$$

$$\cdot \exp\left(j 2\pi \left(\frac{i_1}{T_1} + \cdots + \frac{i_m}{T_m}\right) t\right).$$
∎

Proof of Lemma 2: Since $y(t)$ is quasi-periodic, it can be expressed as

$$y(t) = \sum_{i_1, \ldots, i_m} Y(i_1, \ldots, i_m)$$

$$\cdot \exp\left(j 2\pi \left(\frac{i_1}{T_1} + \cdots + \frac{i_m}{T_m}\right) t\right).$$

The following definition for $\hat{y}(t_1, \ldots, t_m)$ satisfies $y(t) = \hat{y}(t + c_1, \ldots, t + c_m)$:

$$\hat{y}(t_1, \ldots, t_m)$$
$$= \sum_{i_1, \ldots, i_m} \left[Y(i_1, \ldots, i_m) \right.$$
$$\left. \cdot \exp\left(-j2\pi \left(\frac{i_1 c_1}{T_1} + \cdots + \frac{i_m c_m}{T_m} \right) \right) \right]$$
$$\cdot \exp\left(j2\pi \left(\frac{i_1 t_1}{T_1} + \cdots + \frac{i_m t_m}{T_m} \right) \right).$$

∎

Proof of Theorem 3 (MPDE Necessity Condition): Since $b(t)$ and $x(t)$ are quasi-periodic, they can be expressed in the form

$$b(t) = \sum_{i_1, \ldots, i_m} B(i_1, \ldots, i_m)$$
$$\cdot \exp\left(j2\pi \left(\frac{i_1}{T_1} + \cdots + \frac{i_m}{T_m} \right) t \right)$$
$$x(t) = \sum_{i_1, \ldots, i_m} X(i_1, \ldots, i_m)$$
$$\cdot \exp\left(j2\pi \left(\frac{i_1}{T_1} + \cdots + \frac{i_m}{T_m} \right) t \right).$$

Our goal is to construct multivariate versions of these signals such that the multivariate versions satisfy the MPDE. This is straightforward when $(T_1, \ldots, T_m)$ are mutually incommensurate, but requires a little more work when they are commensurately related. We start by defining $\hat{b}(t_1, \ldots, t_m)$ and $\hat{x}(t_1, \ldots, t_m)$ by

$$\hat{b}(t_1, \ldots, t_m) = \sum_{i_1, \ldots, i_m} \hat{B}(i_1, \ldots, i_m)$$
$$\cdot \exp\left(j2\pi \left(\frac{i_1 t_1}{T_1} + \cdots + \frac{i_m t_m}{T_m} \right) \right)$$
$$\hat{B}(i_1, \ldots, i_m) = B(i_1, \ldots, i_m)$$
$$\cdot \exp\left(-j2\pi \left(\frac{i_1 c_1}{T_1} + \cdots + \frac{i_m c_m}{T_m} \right) \right)$$
$$\hat{x}(t_1, \ldots, t_m) = \sum_{i_1, \ldots, i_m} \hat{X}(i_1, \ldots, i_m)$$
$$\cdot \exp\left(j2\pi \left(\frac{i_1 t_1}{T_1} + \cdots + \frac{i_m t_m}{T_m} \right) \right)$$
$$\hat{X}(i_1, \ldots, i_m) = X(i_1, \ldots, i_m)$$
$$\cdot \exp\left(-j2\pi \left(\frac{i_1 c_1}{T_1} + \cdots + \frac{i_m c_m}{T_m} \right) \right).$$

Note, that $x(t) = \hat{x}(t + c_1, \ldots, t + c_m), b(t) = \hat{b}(t + c_1, \ldots, t + c_m)$. Now define $\hat{Q}(i_1, \ldots, i_m)$ and $\hat{F}(i_1, \ldots, i_m)$ by

$$\sum_{i_1, \ldots, i_m} \hat{Q}(i_1, \ldots, i_m) \exp\left(j2\pi \left(\frac{i_1 t_1}{T_1} + \cdots + \frac{i_m t_m}{T_m} \right) \right)$$
$$= \hat{q}(t_1, \ldots, t_m) = q(\hat{x}(t_1, \ldots, t_m))$$

$$\sum_{i_1, \ldots, i_m} \hat{F}(i_1, \ldots, i_m) \exp\left(j2\pi \left(\frac{i_1 t_1}{T_1} + \cdots + \frac{i_m t_m}{T_m} \right) \right)$$
$$= \hat{f}(t_1, \ldots, t_m) = f(\hat{x}(t_1, \ldots, t_m)).$$

Noting that $b(t) = \hat{b}(t + c_1, \ldots, t + c_m)$ and $x(t) = \hat{x}(t + c_1, \ldots, t + c_m)$ and inserting $x(t)$ into (5), the following equality is obtained:

$$\sum_{i_1, \ldots, i_m} \left[j2\pi \left(\frac{i_1}{T_1} + \cdots + \frac{i_m}{T_m} \right) \hat{Q}(i_1, \ldots, i_m) \right.$$
$$\left. - \hat{F}(i_1, \ldots, i_m) - \hat{B}(i_1, \ldots, i_m) \right]$$
$$\cdot \exp\left(j2\pi \left(\frac{i_1}{T_1} + \cdots + \frac{i_m}{T_m} \right) t \right) = 0.$$

When $T_1, \ldots, T_m$ are pairwise incommensurate, each term in the above summation can be equated to zero. In general, however, the functions $e^{j2\pi((i_1/T_1) + \cdots + (i_m/T_m))t}$ can be linearly dependent, so we have to generalize this idea. We will proceed by collecting together terms in the summation that are linearly dependent. More precisely, if $T_1, \ldots, T_m$ are mutually commensurate, then the map

$$\mathcal{M}: \{(i_1, \ldots, i_m)\} \mapsto \left\{ 2\pi \left(\frac{i_1}{T_1} + \cdots + \frac{i_m}{T_m} \right) \right\}$$

(i.e., the map from the indices to the frequencies) is many-to-one instead of one-to-one. Denote the range of $\mathcal{M}$ by Ω, consisting of a countable set of distinct frequencies ω_k. For any $\omega_k \in \Omega$, define I_k to be the set of all indices $(i_1, \ldots, i_m)$ such that

$$\omega_k = 2\pi \left(\frac{i_1}{T_1} + \cdots + \frac{i_m}{T_m} \right)$$

i.e., $I_k = \mathcal{M}^{-1}(\omega_k)$. If $T_1, \ldots, T_m$, are mutually incommensurate, then I_k has exactly one member; otherwise, it is a countably infinite set. The important property resulting from this definition is that if $\omega_k \neq \omega_l$, then $I_k \cap I_l = \emptyset$.

The DAE above can now be rewritten as

$$\sum_k \left[\sum_{(i_1, \ldots, i_m) \in I_k} \left[j2\pi \left(\frac{i_1}{T_1} + \cdots + \frac{i_m}{T_m} \right) \hat{Q}(i_1, \ldots, i_m) \right. \right.$$
$$\left. \left. - \hat{F}(i_1, \ldots, i_m) - \hat{B}(i_1, \ldots, i_m) \right] \right] e^{j\omega_k t} = 0.$$

By the above construction, we are now guaranteed that the functions $e^{j\omega_k t}$ are linearly independent, hence their coefficients must be zero:

$$\sum_{(i_1, \ldots, i_m) \in I_k} \left[j2\pi \left(\frac{i_1}{T_1} + \cdots + \frac{i_m}{T_m} \right) \hat{Q}(i_1, \ldots, i_m) \right.$$
$$\left. - \hat{F}(i_1, \ldots, i_m) - \hat{B}(i_1, \ldots, i_m) \right] = 0.$$

(31)

Equation (31) is equivalent to requiring the DAE to be satisfied. The requirement for the MPDE to be satisfied is, however,

stronger: each term in the summation above must individually equal zero. In general, this latter condition will not be met by the $\hat{X}$ and $\hat{B}$ defined above.

We can, however, take advantage of the fact that in the commensurate case, many (in fact uncountably many) different choices of multivariate forms for $\hat{b}$ and $\hat{x}$ correspond to the same univariate function. From among these, we will choose new multivariate forms for $\hat{x}$ and $\hat{b}$ in such a way that not only is (31) satisfied, but the stronger condition that each term in the summation is zero is also satisfied.

We actually keep the same $\hat{x}$ defined earlier, but make a new choice for the excitation $\hat{b}$ by defining a new set of quasi-periodic excitation coefficients $\tilde{B}(i_1, \ldots, i_m)$, and corresponding excitation $\tilde{b}(t)$, as follows:

$$
\tilde{B}(i_1, \ldots, i_m) = \left[j2\pi \left(\frac{i_1}{T_1} + \cdots + \frac{i_m}{T_m} \right) \hat{Q}(i_1, \ldots, i_m) \right.
$$

$$
\left. - \hat{F}(i_1, \ldots, i_m) \right]
$$

$$
\cdot \exp \left(j2\pi \left(\frac{i_1 c_1}{T_1} + \cdots + \frac{i_m c_m}{T_m} \right) \right).
$$
(32)

Note, that from definition, $\tilde{B}(i_1, \ldots, i_m)$ satisfy (31), hence $\tilde{b}(t)$ and $x(t)$ together satisfy the DAE.

Now, define $\hat{\tilde{b}}(t_1, \ldots, t_m)$ by

$$
\hat{\tilde{b}}(t_1, \ldots, t_m) = \sum_{i_1, \ldots, i_m} \hat{\tilde{B}}(i_1, \ldots, i_m)
$$

$$
\exp \left(j2\pi \left(\frac{i_1 t_1}{T_1} + \cdots + \frac{i_m t_m}{T_m} \right) \right),
$$

$$
\hat{\tilde{B}}(i_1, \ldots, i_m) = \tilde{B}(i_1, \ldots, i_m)
$$

$$
\exp \left(-j2\pi \left(\frac{i_1 c_1}{T_1} + \cdots + \frac{i_m c_m}{T_m} \right) \right).
$$

Note, that from this definition, $\tilde{b}(t) = \hat{\tilde{b}}(t + c_1, \ldots, t + c_m)$ is

$$
\tilde{b}(t) = \sum_{\substack{k \\ (i_1, \ldots, i_m) \in I_k}}
$$

$$
\cdot \left[j2\pi \left(\frac{i_1}{T_1} + \cdots + \frac{i_m}{T_m} \right) \hat{Q}(i_1, \ldots, i_m) \right.
$$

$$
\left. - \hat{F}(i_1, \ldots, i_m) \right] e^{j\omega_k t}.
$$

Using (31) and (32), this simplifies to

$$
\tilde{b}(t) = \sum_{\substack{k \\ (i_1, \ldots, i_m) \in I_k}} \hat{B}(i_1, \ldots, i_m) e^{j\omega_k t}
$$

$$
= \sum_{i_1, \ldots, i_m} \hat{B}(i_1, \ldots, i_m)
$$

$$
\cdot \exp \left(j2\pi \left(\frac{i_1}{T_1} + \cdots + \frac{i_m}{T_m} \right) t \right) = b(t).
$$

Hence, $\hat{\tilde{b}}(t + c_1, \ldots, t + c_m) = b(t)$. Finally, it needs to be shown that $\hat{\tilde{b}}(t_1, \ldots, t_m)$ and $\hat{x}(t_1, \ldots, t_m)$ satisfy the MPDE. On substituting the expressions for these multivariate functions into the MPDE, the following equation is obtained:

$$
\sum_{i_1, \ldots, i_m} \left[j2\pi \left(\frac{i_1}{T_1} + \cdots + \frac{i_m}{T_m} \right) \hat{Q}(i_1, \ldots, i_m) \right.
$$

$$
\left. - \hat{F}(i_1, \ldots, i_m) - \hat{\tilde{B}}(i_1, \ldots, i_m) \right]
$$

$$
\cdot \exp \left(j2\pi \left(\frac{i_1 t_1}{T_1} + \cdots + \frac{i_m t_m}{T_m} \right) \right) = 0.
$$

From the definition of $\hat{\tilde{B}}(i_1, \ldots, i_m)$, the coefficients of the above expression are zero, hence the theorem is proved. ∎

Proof of Theorem 4 (Uniqueness of Envelope): The proof rests on the fact that the solutions of the MPDE along "diagonal" lines $(t, t + c_2, \ldots, t + c_m)$ in the $t_1, \ldots, t_m$ space are exactly the solution of the circuit DAE with the initial condition $h(c_2, \ldots, c_m)$. This follows from Theorem 1. On the diagonal lines passing through each point $(0, c_2, \ldots, c_m)$ in the initial condition region $0 \times \prod_{i=2}^{m} [0, T_i]$, therefore, the MPDE has a unique solution, since the DAE has a unique solution with initial condition $h(c_2, \ldots, c_m)$. The diagonal lines are illustrated for the two-rate case by the shaded area in Fig. 10(a). Since $\hat{x}$ is periodic with respect to $t_2, \ldots, t_m$, its value at any point $(t_1, \ldots, t_m)$ is equal to that at some point along one of the diagonal lines above. This is illustrated in Fig. 10(b). Hence $\hat{x}(t_1, \ldots, t_m)$ is uniquely specified. ∎

REFERENCES

[1] L. W. Nagel, "SPICE2: A computer program to simulate semiconductor circuits," Ph.D. dissertation, Electr. Electron. Comp. Sci. Dept., Univ. Calif. Berkeley, Elec. Res. Lab., 1975.

[2] T. Quarles, "Analysis of performance and convergence issues for circuit simulation," Ph.D. dissertation, Electr. Electron. Comp. Sci. Dept., Univ. Calif. Berkeley, Elec. Res. Lab., Apr. 1989.

[3] J. Roychowdhury, "Reduced-order modeling of time-varying systems," *IEEE Trans. Circuits Syst. II*, vol. 46, no. 10, Nov. 1999.

[4] O. Narayan and J. Roychowdhury, "Multi-time simulation of voltage-controlled oscillators," in *Proc. IEEE DAC'99*, New Orleans, LA, June 1999.

[5] J. Kevorkian and J. D. Cole, *Perturbation Methods in Applied Mathematics*. New York: Springer-Verlag, 1981.

[6] E. Ngoya and R. Larchevèque, "Envelop transient analysis: A new method for the transient and steady state analysis of microwave communication circuits and systems," in *Proc. IEEE MTT Symp.*, 1996.

[7] H. Brachtendorf, G. Welsch, R. Laur, and A. Bunse-Gerstner, "Numerical steady state analysis of electronic circuits driven by multi-tone signals," in *Electrical Engineering*. New York: Springer-Verlag, 1996, vol. 79, pp. 103–112.

[8] K. Kundert, J. K. White, and A. Sangiovanni-Vincentelli, *Steady-State Methods for Simulating Analog and Microwave Circuits*. Norwell, MA: Kluwer, 1990.

[9] R. Melville, P. Feldmann, and J. Roychowdhury, "Efficient multi-tone distortion analysis of analog integrated circuits," in *Proc. IEEE CICC*, May 1995, pp. 241–244.

[10] R. J. Gilmore and M. B. Steer, "Nonlinear circuit analysis using the method of harmonic balance—A review of the art—Part I. Introductory concepts," *Int. J. Microwave Millimeter Wave CAE*, vol. 1, no. 1, 1991.

[11] M. Rösch and K. J. Antreich, "Schnell stationäre simulation nicht-linearer schaltungen im frequenzbereich," *AEÜ*, vol. 46, no. 3, pp. 168–176, 1992.

[12] D. Sharrit, "New method of analysis of communication systems," in *Proc. MTTS WMFA: Nonlinear CAD Workshop*, June 1996.

[13] P. Feldmann and J. Roychowdhury, "Computation of circuit waveform envelopes using an efficient, matrix-decomposed harmonic balance algorithm," in *Proc. ICCAD*, Nov. 1996.

[14] L. O. Chua and A. Ushida, "Algorithms for computing almost periodic steady-state response of nonlinear systems to multiple input frequencies," *IEEE Trans. Circuits. Syst.*, vol. CAS-28, no. 10, pp. 953–971, Oct. 1981.

[15] K. Kundert, J. White, and A. Sangiovanni-Vincentelli, "A mixed frequency-time approach for distortion analysis of switching filter circuits," *IEEE J. Solid-State Circuits*, vol. 24, no. 2, pp. 443–451, Apr. 1989.

[16] M. Farkas, *Periodic Motions*.   New York: Springer-Verlag, 1994.

[17] E. L. Allgower and K. Georg, *Numerical Continuation Methods*.   New York: Springer-Verlag, 1990.

[18] Y. Saad, *Iterative Methods for Sparse Linear Systems*.   Boston, MA: PWS-Kent, 1996.

[19] R. Telichevesky, K. Kundert, and J. White, "Efficient steady-state analysis based on matrix-free Krylov subspace methods," in *Proc. IEEE DAC*, 1995, pp. 480–484.

[20] T. J. Aprille and T. N. Trick, "Steady-state analysis of nonlinear circuits with periodic inputs," *Proc. IEEE*, vol. 60, pp. 108–114, Jan. 1972.

[21] S. Skelboe, "Computation of the periodic steady-state response of non-linear networks by extrapolation methods," *IEEE Trans. Circuits Syst.*, vol. CAS-27, pp. 161–175, Mar. 1980.

Jaijeet Roychowdhury received the Bachelor's degree in electrical engineering from the Indian Institute of Technology, Kanpur, India, in 1987, and the Ph.D. degree in electrical engineering from the University of California, Berkeley, in 1993.

From 1993 to 1995, he was with the CAD Lab of AT&T's Bell Laboratories, Allentown, PA. From 1995 to 2000, he was with the Communication Sciences Research Division of Lucent's Bell Laboratories in Murray Hill, NJ. Currently, he is with CeLight, Inc., Springfield, NJ. His professional interests lie in the design and simulation of electronic and electro-optical systems.